

# Rapid radiation in a highly diverse marine environment

Kosmas Hench<sup>a,1</sup> , Martin Helmkamp<sup>a</sup> , W. Owen McMillan<sup>b</sup> , and Oscar Puebla<sup>a,b,c,d,1</sup> 

<sup>a</sup>Ecology Department, Leibniz Centre for Tropical Marine Research, 28359 Bremen, Germany; <sup>b</sup>Smithsonian Tropical Research Institute, Apartado Postal 0843-03092, Republic of Panama; <sup>c</sup>Institute for Chemistry and Biology of the Marine Environment, 26111 Oldenburg, Germany; and <sup>d</sup>Marine Evolutionary Ecology, GEOMAR Helmholtz Centre for Ocean Research Kiel, 24105 Kiel, Germany

Edited by Nancy Knowlton, National Museum of Natural History, Smithsonian Institution, Washington, DC; received September 30, 2020; accepted November 18, 2021

**Rapid diversification is often observed when founding species invade isolated or newly formed habitats that provide ecological opportunity for adaptive radiation. However, most of the Earth's diversity arose in diverse environments where ecological opportunities appear to be more constrained. Here, we present a striking example of a rapid radiation in a highly diverse marine habitat. The hamlets, a group of reef fishes from the wider Caribbean, have radiated into a stunning diversity of color patterns but show low divergence across other ecological axes. Although the hamlet lineage is ~26 My old, the radiation appears to have occurred within the last 10,000 generations in a burst of diversification that ranks among the fastest in fishes. As such, the hamlets provide a compelling backdrop to uncover the genomic elements associated with phenotypic diversification and an excellent opportunity to build a broader comparative framework for understanding the drivers of adaptive radiation. The analysis of 170 genomes suggests that color pattern diversity is generated by different combinations of alleles at a few large-effect loci. Such a modular genomic architecture of diversification has been documented before in *Heliconius* butterflies, capuchino finches, and munia finches, three other tropical radiations that took place in highly diverse and complex environments. The hamlet radiation also occurred in a context of high effective population size, which is typical of marine populations. This allows for the accumulation of new variants through mutation and the retention of ancestral genetic variation, both of which appear to be important in this radiation.**

adaptive radiation | genomic architecture | marine | *Hypoplectrus* | reef fishes

**A**daptive radiation is driven by ecological opportunity, whereby newly accessible niches provide potential for diversification (1). This process often takes place in geographically isolated and/or newly formed habitats such as lakes or oceanic islands, where founding species are exposed to depauperate environments in which competition is relaxed. This is, for example, the case in exemplary adaptive radiations, like Darwin's finches (2), East African cichlids (3, 4), and Caribbean *Anolis* lizards (5). Nevertheless, these radiations represent extremes of an evolutionary process that may also operate in diverse and complex habitats, where the relationship between biotic and abiotic drivers and rapid speciation is often more subtle. Unfortunately, with the notable exception of *Heliconius* butterflies (6), these radiations remain poorly explored despite the fact that they occur in environments that contain most of the diversity on Earth. As a result, we lack a broader comparative framework for identifying and generally understanding the main drivers of adaptive radiation.

The hamlets (*Hypoplectrus* spp., Serranidae), a group of reef fishes from the wider Caribbean, present an excellent opportunity to investigate the genomic basis of radiation in diverse and complex environments where most niches are already occupied. Typical of marine species (7), most hamlets are characterized by extensive geographic ranges, large population sizes, high fecundity, and high potential for dispersal through a 3-wk pelagic larval stage (8–10). These characteristics are expected to shape their evolutionary potential in complex

ways, possibly reducing the opportunity for speciation (11, 12). Against this backdrop, the genus diversified into at least 18 species that are highly sympatric (9, 13) and very similar in terms of habitat and diet (14, 15). They differ essentially in color pattern, a trait that is thought to be ecologically relevant through crypsis and mimicry (16–20). According to the aggressive mimicry hypothesis, some hamlet species (the mimics) achieve higher preying success by resembling other fishes from different families (the models) that are harmless to the hamlets' prey. In agreement with this hypothesis, behavioral differences in resource acquisition have been documented between hamlet species (19, 20). Yet, resemblance between models and mimics is imperfect, and some species appear to be neither cryptic nor mimetic. Color pattern is an important cue for mate choice, and hamlets show strong assortative mating both in the field and in the laboratory (10, 13, 18, 19, 21). In addition, hamlets are simultaneously hermaphroditic, and mate choice is mutual (8, 22). This particular mating system results in complex pairing dynamics among individuals that can contribute to diversification by generating strong sexual selection (13, 23). Despite strong assortative mating, interspecific spawnings are occasionally observed in natural populations (10, 13, 18, 19, 21). Fertilization is external, and eggs are planktonic. The available evidence suggests that there are no barriers to fertilization among species (24) and that gene flow is ongoing (25). Genetically, the Caribbean hamlets are very closely related. Similar to East

## Significance

**Adaptive radiation, the evolutionary process whereby a lineage diversifies over a short period of time, often occurs in geographically isolated or newly formed habitats where colonizing species encounter unoccupied niches and reduced selective pressures. Rapid radiations may also occur in diverse and complex environments, but these cases are less well documented. Here, we show that the hamlets, a group of Caribbean reef fishes, radiated within the last 10,000 generations in a burst of diversification that ranks among the fastest in fishes. Genomic analysis suggests that color pattern diversity is generated by different combinations of alleles at a few genes with large effect. Such a modular genomic architecture of diversification is emerging as a common denominator to a variety of radiations.**

Author contributions: K.H., M.H., W.O.M., and O.P. designed research; K.H., M.H., and O.P. performed research; K.H., M.H., and O.P. analyzed data; and K.H., M.H., W.O.M., and O.P. wrote the paper.

The authors declare no competing interest.

This article is a PNAS Direct Submission.

This article is distributed under [Creative Commons Attribution-NonCommercial-NoDerivatives License 4.0 \(CC BY-NC-ND\)](https://creativecommons.org/licenses/by-nc-nd/4.0/).

<sup>1</sup>To whom correspondence may be addressed. Email: k.hench@posteo.de or oscar.puebla@leibniz-zmt.de.

This article contains supporting information online at <https://www.pnas.org/lookup/suppl/doi:10.1073/pnas.2020457119/-DCSupplemental>.

Published January 18, 2022.

African cichlids from Lake Victoria (4), they show generally low levels of genetic divergence (13, 21, 25–27) and do not sort into distinct mitochondrial haplogroups (28–30). A chromosome-resolution reference genome is now available for the group (25), which provides the foundation to more fully explore the genomic basis of this radiation. Here, we examine the genomes of 170 individuals from 28 pairs of sympatric species to 1) uncover the genomic architecture of the radiation, 2) identify genomic regions associated with major phenotypic differences, and 3) ask how the hamlet radiation compares with other rapid radiations.

## Results

**Rapid Radiation, Old Lineage.** We started by considering the hamlet radiation in the context of the phylogeny of the subfamily Serraninae and the Fish Tree of Life (FToL) estimates of evolutionary rates (31). This broad phylogenetic perspective indicates that the hamlets exhibit speciation rates that are among the highest in fishes (mean clade-specific speciation rate: 2.44) (*SI Appendix, Fig. S1*). Within the Serraninae, a single burst of diversification was identified at the base of the hamlet radiation (Fig. 1A and *SI Appendix, Fig. S2*). No other serranine lineage radiated rapidly (subfamily background speciation rate excluding hamlets: 0.11). Notably, this includes the chalk bass (*Serranus tortugarum*) and the tobaccifish

(*Serranus tabacarius*), two species that are closely related to the hamlets and have a similar mating system (33). The two clades that are simultaneously hermaphroditic (marked by a star in Fig. 1A and *SI Appendix, Fig. S2A*) do not present an increase in diversification rate either. Finally, the time-calibrated FToL phylogeny illustrates that although the extant hamlet species appear to be very young, the *Hypoplectrus* lineage last shared a common ancestor with other species in the subfamily ~26 Mya (*SI Appendix, Fig. S2A*).

**Population Genetic Patterns.** Given the low levels of genetic divergence among hamlets, we first used our genomic data from Belize, Honduras, and Panama to examine to what extent sympatric hamlets represent genetic clusters. Principal component analysis indicates that this is generally the case, albeit with varying degrees of overlap between species (Fig. 1C–E). We next grouped samples from each species and location together to examine patterns of genome-wide differentiation ( $F_{ST}$ ) between pairs of sympatric species. This analysis reveals a continuous range of differentiation, from <0.003 to 0.1 (Fig. 1B and *SI Appendix, Table S1*). It is important to stress that this differentiation continuum does not constitute a temporal sequence of speciation, as it includes different species from different locations. Moreover, the barred, black, and butter hamlets are over-represented in this dataset since they were sampled at the three

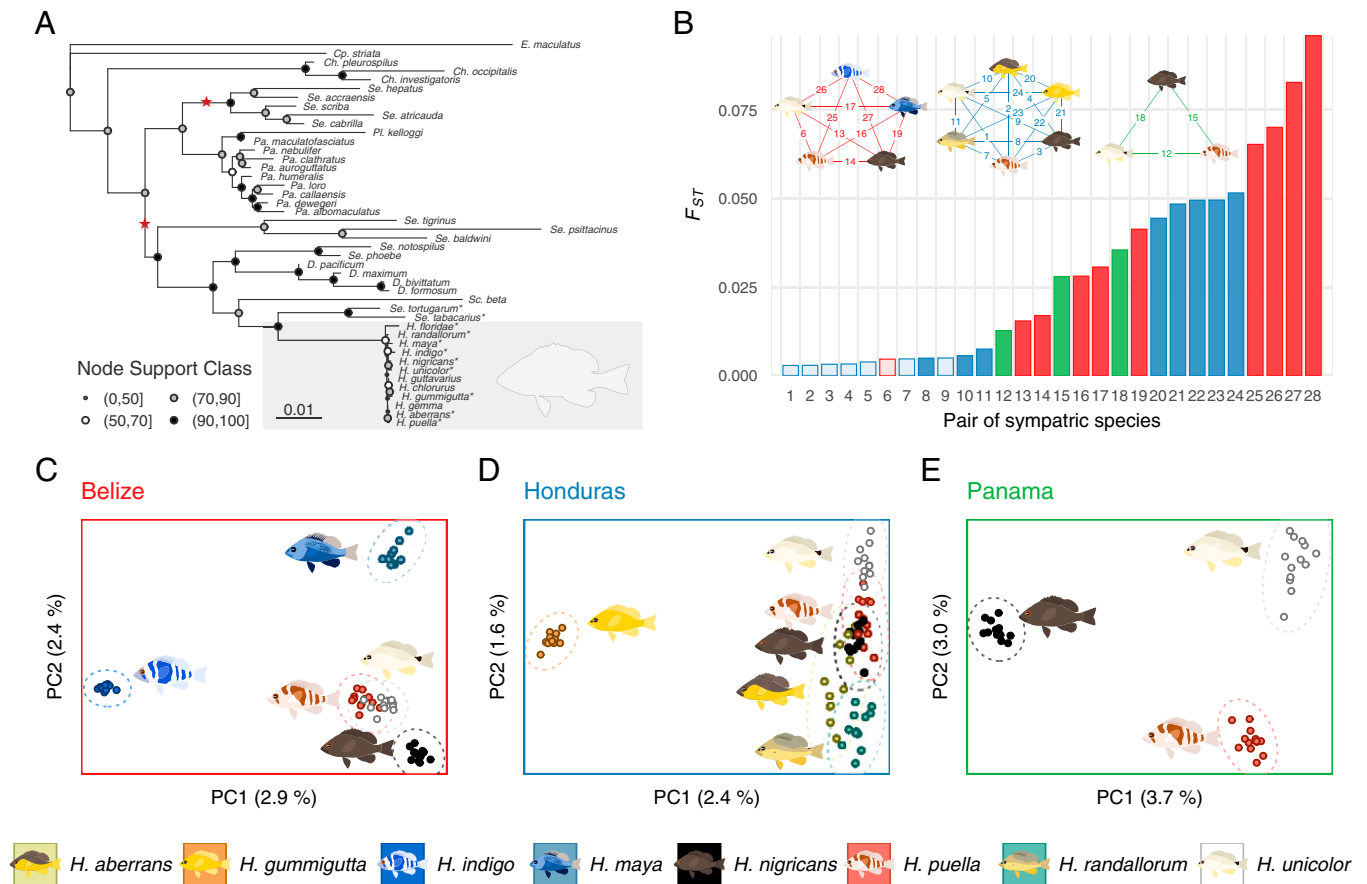


**Fig. 1.** Phylogenetic context and population genetic patterns. (A) Maximum likelihood phylogeny of the Serraninae subfamily based on 23 nuclear and mitochondrial genes. The hamlet radiation is highlighted in gray, and species considered in this study are marked with an asterisk. Gene sequences for the other species were obtained from the FToL project (31). Stars denote clades that are simultaneously hermaphroditic following ref. 32 (note that the mating system of *Serranus accraensis* is not known). *Ch.*, *Chelidoperca*; *Cp.*, *Centropristis*; *D.*, *Diplectrum*; *E.*, *Epinephelus*; *H.*, *Hypoplectrus*; *Pa.*, *Paralabrax*; *Pl.*, *Plectranthias*; *Sc.*, *Schultzzea*; *Se.*, *Serranus*. (B) Genetic differentiation ( $F_{ST}$ ) between pairs of sympatric hamlets. The 28 pairs are numbered and presented in order of increasing genome-wide differentiation, and they are color coded with respect to location (red, Belize; blue, Honduras; green, Panama). The pairs that are significantly differentiated at the  $\alpha = 0.05$  level are highlighted with filled bars. (C–E) Principal component analysis (PCA) for each location. The percentage of variation explained by each principal component (PC) is shown. The PCAs were repeated with the highly diverged genomic regions excluded and produced very similar results (*SI Appendix, Fig. S3*), indicating that the clustering patterns are not driven by these regions.

locations. Nevertheless, levels of genetic differentiation among populations within species are within the range of differentiation between sympatric species (*SI Appendix, Table S1*). From a population genetic perspective, populations of the same species can, therefore, be as distinct as different species (34, 35).

**Genomic Architecture of Radiation.** We then divided the genome into 50-kb windows to reveal how the genomic architecture of the hamlet radiation unfolds across the differentiation continuum. The radiation is characterized by a small number of sharp peaks [so-called “islands” (36)] of differentiation that do not expand with increasing genome-wide differentiation (Fig. 2*A* and *SI Appendix, Figs. S4 and S5*). Their number does not increase substantially either, with  $\leq 6$  peaks with  $F_{ST} > 0.7$  per species pair throughout the entire continuum. It is also noteworthy that at the lower end of the differentiation continuum, differentiation is largely independent from recombination rate (*SI Appendix, Fig. S6A*, row 1). In this respect, our results contrast with previous studies conducted across higher levels of differentiation that report a marked effect of recombination on differentiation (37–41). We nonetheless capture the onset of the effect of recombination, with differentiation accumulating disproportionately in regions of low recombination as genome-wide differentiation increases (*SI Appendix, Fig. S6*). This effect is particularly strong in a large section of linkage group (LG) (chromosome) 8, which we had previously identified as a low-recombining region (25, 42) (Fig. 2*A*). In contrast to genetic differentiation ( $F_{ST}$ , which captures allele frequency differences), the genomic architecture of divergence ( $d_{XY}$ , which captures sequence divergence) is similar across all species pairs (*SI Appendix, Fig. S7*). Divergence is generally elevated in the chromosome peripheries where recombination rate tends to be higher (*SI Appendix, Fig. S8B and D*). This is likely an effect of the recombination landscape that shaped ancestral variation, resulting in higher diversity in regions of high recombination

(*SI Appendix, Fig. S9*). In order to filter out the effect of ancestral diversity from the divergence signal, we considered the range of divergence among species pairs, which we defined as  $\Delta d_{XY} = \max(d_{XY}) - \min(d_{XY})$  among the 28 pairs. This statistic varied markedly along the genome (*SI Appendix, Fig. S8E*), paralleling in part patterns of genetic differentiation (Fig. 2*A*) and indicating heterogeneous selection among species at these loci. Divergence between species is also strongly correlated with nucleotide diversity ( $\pi$ ) within species (*SI Appendix, Fig. S10*), which is in line with the theoretical expectation that  $d_{XY}$  approaches ancestral diversity when divergence is very recent (43).

**Recent Radiation.** In order to estimate the age of the hamlet radiation, we inferred the demographic histories of all species in all locations using the multiple sequentially Markovian coalescent (MSMC2) (44). The cross-coalescence patterns suggest that hamlets diverged within the last 10,000 generations (Fig. 3*B*). These results are consistent with previous analyses using a different approach that does not rely on phasing (45). Alternatively, gene flow among sympatric species may have obliterated the signature of older demographic events, which could be complex and involve several cycles of “fission–fusion–fission” (46). Nevertheless, reconstructing such events is challenging at the low levels of divergence that characterize the Caribbean hamlets. The MSMC2 analyses also indicate that ancestral effective population sizes remained high, in the order of  $10^4 - 10^5$  (Fig. 3*A*).

**Ongoing Gene Flow and Introgression.** The overall landscape of genomic differentiation suggests that it is shaped in part by gene flow and introgression. In order to test for ongoing gene flow, we searched for genetic hybrids and backcrosses in our dataset. A total of 12 high-probability hybrids and backcrosses were identified (*SI Appendix, Fig. S11*), representing 7% of the individuals analyzed. This proportion is likely an underestimate since our sampling design explicitly excluded individuals with intermediate color patterns. It is also substantially higher than

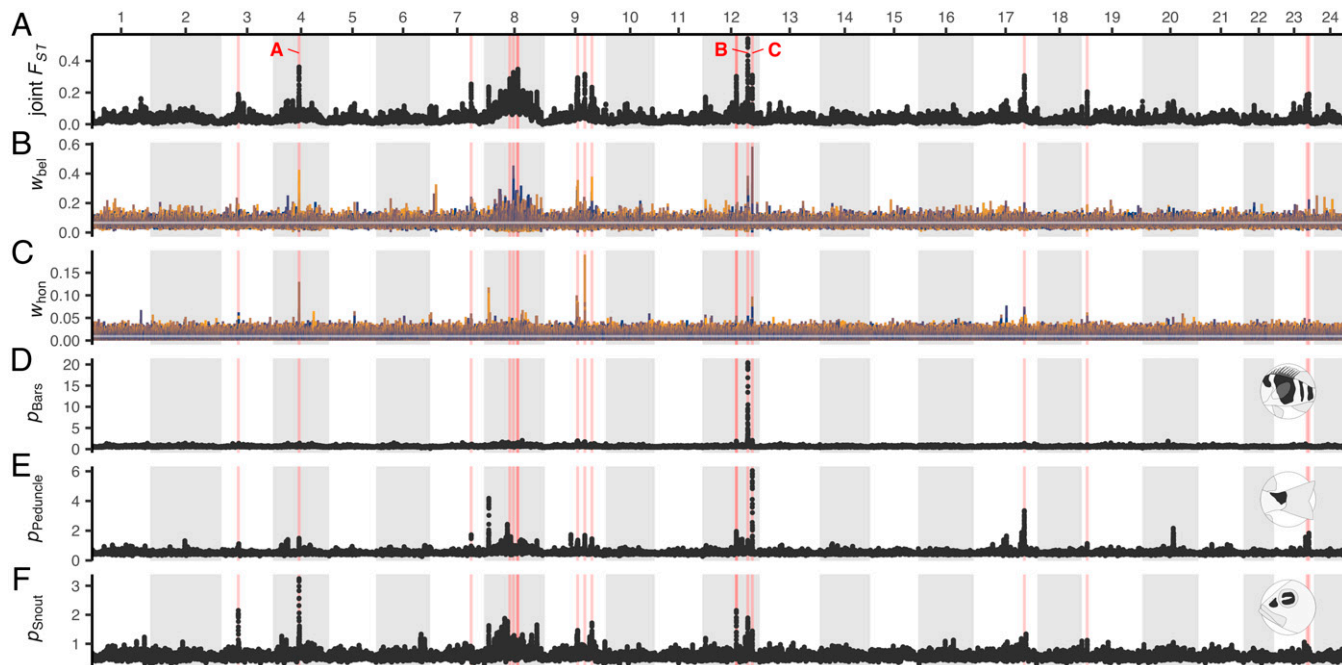


**Fig. 2.** Whole-genome patterns. The alternating white and gray blocks represent the 24 LGs (chromosomes). All statistics are calculated over 50-kb sliding windows with 5-kb increments unless stated otherwise. (A) Joint differentiation ( $F_{ST}$ ) among the 14 groups of samples (species within locations). The red vertical lines highlight regions above the 99.8th  $F_{ST}$  percentile (*SI Appendix, Table S2*). Letters A, B, and C correspond to the three genomic regions that are highlighted in Fig. 5. (B and C) Topology weighting for Belize and Honduras, respectively, along nonoverlapping 200 SNP windows. The different colors correspond to different topologies, and the white horizontal lines indicate the null weighting (i.e., all topologies equally likely). (D–F)  $G \times P$  association for bars, dark saddle on the caudal peduncle, and spot on the snout, respectively. An expanded version of this figure is presented in *SI Appendix, Fig. S8*.

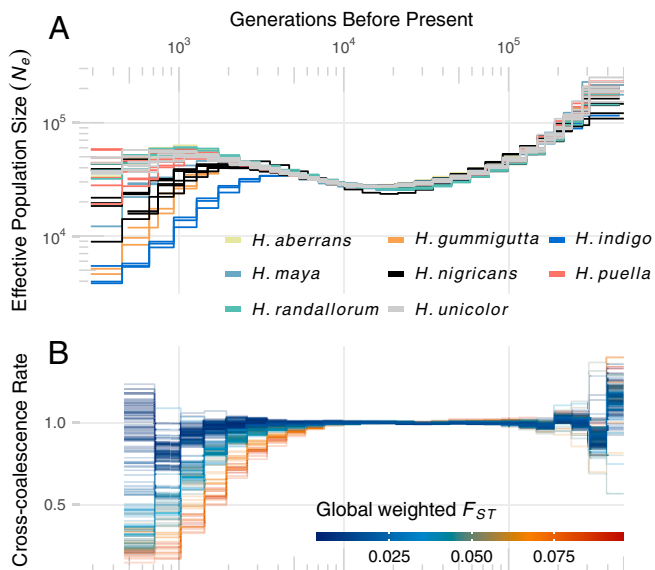


**Fig. 3.** Demographic inference. (A) Inferred history of effective population size. Each line is based on three to four genomes per group (species within locations). (B) Cross-coalescence rates for the 28 pairs of sympatric species color coded by genome-wide  $F_{ST}$ . Each line represents an independent run based on two genomes from two sympatric species (total of four). A cross-coalescence rate of one indicates completely shared ancestry, and a rate of zero indicates no shared ancestry. All estimates are scaled with a per site mutation rate  $\mu = 3.7 \times 10^{-8}$ . The most ancient and the two most recent time segments are omitted due to unreliable inference at these extremes.

the 2% interspecific spawnings that were observed at the three locations (13, 19). However, behavioral observations indicate that hybridization rate can vary dramatically in the hamlets depending on the social context of individuals at the time of spawning (13).

In order to test for past introgression events, we calculated  $D$  statistics for all possible trios of species/populations using *Hypoplectrus floridae*—which belongs to the Gulf of Mexico hamlet clade (47)—as the out-group. In the most treelike configuration (BBAA), a total of 69 trios show evidence of introgression, representing 19% of the 364 trios that we tested. This proportion is slightly higher than the 14% reported in East African cichlids from Lake Victoria (4). Importantly, all species/populations and 44% of all pairs show evidence of introgression (SI Appendix, Fig. S12), indicating that it is pervasive across the radiation.

**Weak Background Phylogenetic Signal.** The low levels of divergence, ongoing gene flow, and history of extensive introgression observed in the hamlets are expected to obscure—possibly even rewrite—the phylogenetic relationships among species and populations. As a result, the genome-wide phylogeny of the radiation is not well resolved, particularly with respect to the deeper nodes of the tree (Fig. 4A). The reconstruction only recovers the most differentiated species (*Hypoplectrus indigo*, *Hypoplectrus gummigutta*, and *Hypoplectrus maya*) as monophyletic. High levels of discordance among genomic regions suggest that lack of divergence and nontree-like evolutionary processes have prevented the buildup of sufficient phylogenetic signal to resolve the relationships among the other species. While most deeper splits thus remain ambiguous, the analysis implies that several species are polyphyletic, including *Hypoplectrus randallorum* and the widely distributed barred (*Hypoplectrus puella*) and butter (*Hypoplectrus unicolor*) hamlets. These patterns are also reflected in a network representation of the genomic data based on fragments of identity by descent (IBD) (Fig. 4B and SI Appendix, Fig. S13). Here, phylogenetically well-resolved clades form tightly linked

clusters, whereas unsupported groups appear diffuse and weakly connected. Several subnetworks across species boundaries also emerge from the network, consistent with a history of rapid divergence and introgression.

**Genetic Basis of Phenotypic Diversification.** The weak phylogenetic signal in the hamlets provides the context to localize regions of the genome that are likely responsible for phenotypic differences among species. The underlying logic is that functionally important regions should group individuals by phenotype. We used topology weighting by iterative sampling of subtrees [Twisst (48)] to dissect the phylogenetic signal along the genome. Briefly, this method considers sliding-windows phylogenies along the genome and weights the contribution of each possible taxon topology to the full tree. As expected given the weak phylogenetic signal in the hamlets and the small size of the windows considered (200 single-nucleotide polymorphism [SNPs]), this approach failed to identify a leading taxon topology at most windows throughout the genome. Nevertheless, it revealed a number of sharp topology weighting peaks (Fig. 2B and C). For example, in Belize, the topologies in which *H. indigo* and *H. maya*—the two blue hamlet species—are sister species dominate a narrow region on LG 4 (Fig. 5A), while two other regions on LG 12 are dominated by topologies grouping the two hamlet species that display vertical bars (*H. indigo* and *H. puella*) (Fig. 5B and C). These patterns are also visible in phylogenies based on the entire contiguous sequence of these regions (SI Appendix, Figs. S14 and S15).

In order to further explore the association between genetic variation and specific components of color pattern, we scored all fishes for the presence or absence of vertical bars, saddle mark on the caudal peduncle, and spot on the snout (SI Appendix, Fig. S16). These traits were chosen because they are polymorphic and can be scored unambiguously. Genotype  $\times$  phenotype ( $G \times P$ ) association analysis revealed a strong association between the presence or absence of vertical bars and genetic variation in a narrow genomic interval on LG 12 (Fig. 2D). Associations with the other two traits were more diffuse, but here again, association peaks emerged, notably on LG 12 for the saddle mark and on LG 4 for the snout spot (Fig. 2E and F). Clustering patterns at these genomic regions (SI Appendix, Fig. S16) are consistent with the topology weighting, phylogenetic, and  $G \times P$  analyses.

The genomic regions identified by topology weighting and  $G \times P$  analyses also match regions of high differentiation ( $F_{ST}$ ) among species (Figs. 2A and 5). Altogether, these analyses allow us to start dissecting the genetic variation associated with phenotypic diversity in the hamlets. The strongest signal was observed in a narrow region of LG 12 that shows a strong association with the presence or absence of vertical bars (letter B in Fig. 2). The 13 pairs of sympatric species that include one species with vertical bars and one without present high differentiation at this locus, while the 15 species pairs that include two species with bars or two species without bars do not (Fig. 5B). In line with this pattern, the region is dominated by topologies in which the two hamlets with vertical bars are sister species. This locus, which we had previously identified (25), is centered on *casz1* (Fig. 5B). This gene encodes a castor zinc finger transcription factor that is involved in a number of processes through development.

Our data also provide insights into the *hoxca* gene cluster on LG 12. In line with our preliminary analyses (25), we observe a strong association between variation at the *hoxc13a* locus and the presence or absence of a saddle mark on the caudal peduncle (Fig. 5C), which is characteristic of the butter hamlet (*H. unicolor*). The pairs of sympatric species that are most differentiated at this locus include *H. unicolor*, and the region is dominated by topologies that single out the butter hamlet. In addition, we observe a secondary association with vertical bars between *hoxc8a*

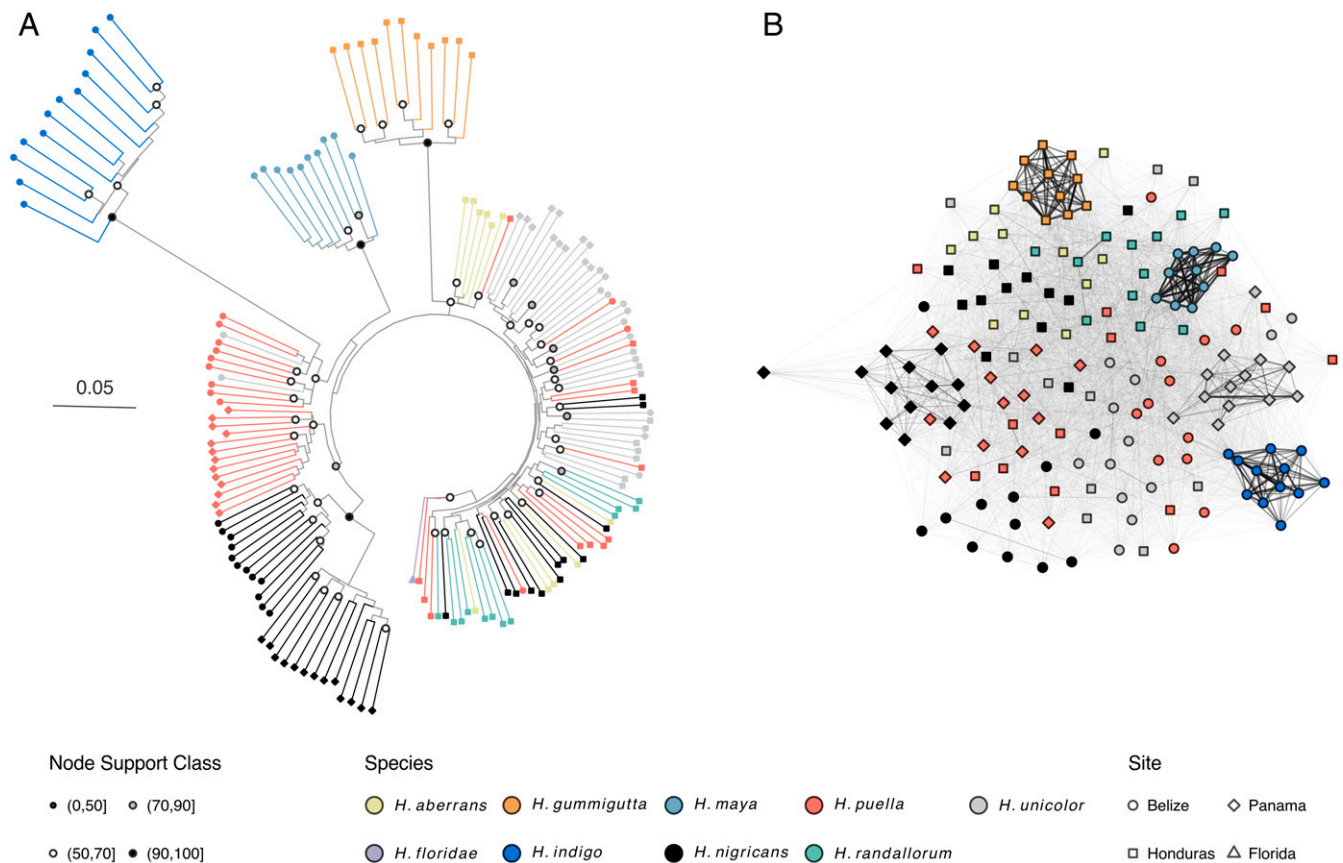


**Fig. 4.** Genome-wide phylogeny and IBD network. (A) Coalescent-based species tree of the Caribbean hamlet samples as inferred from 5,000 local trees of 5-kb windows each randomly distributed throughout the genome. Internal branches are measured in coalescent units, thus reflecting concordance among local trees. Note that terminal branch lengths were set to an arbitrary constant. Support values at the nodes are given as local posterior probabilities. The tree is rooted with *H. floridae* from Florida, a member of the Gulf of Mexico clade. A version rooted with *Serranus* is presented in *SI Appendix, Fig. S17*. (B) IBD network considering IBD fragments larger than 5 and  $10 \times 10^3$  consecutive SNPs for one and two shared haplotypes, respectively, and filtered for a minimum length of 0.2 cM. The distribution of IBD fragments along the genome and the networks for longer IBD fragments are presented in *SI Appendix, Figs. S13 and S18*. Both analyses (phylogeny and IBD network) confirm that the most differentiated species (*H. indigo*, *H. gummigutta*, and *H. maya*) form tight genetic clusters, but they also indicate that low levels of divergence, ongoing gene flow, and pervasive introgression obscure the phylogenetic relationships among the other clades (note the low support values and short branches in the deeper nodes of the tree).

and *hoxc11a*. Hox genes play an important role in patterning tissues along the body axis and have been shown to be involved in color pattern development in insects (49, 50) and vertebrates (51). They are arranged and expressed in a sequence that follows the body axis, with 3' genes expressed anteriorly and 5' genes posteriorly (52). This pattern is consistent with our results as *hoxc13a* is the most 5' gene of the *hoxca* cluster, the saddle on the caudal peduncle is the most posterior mark in the hamlets, and *hoxc13a* is known to be expressed in the caudal peduncle and at the pigment appearance stage in fishes (53, 54). Vertical bars, on the other hand, are anterior to the saddle mark just as the *hoxc8-11a* gene is on the 3' side of *hoxc13a*. A list of the genes found in the 18 genomic regions above the 99.8th  $F_{ST}$  percentile is presented in *SI Appendix, Table S2* and includes a number of genes that are involved in pigmentation/skin development (e.g., *tmem79*, *mafb*, *kitlg*) and vision/photoreceptor development (e.g., *grk7a*, *rab8a*, *slc12a5*). Functional analyses are needed to test the role played by these candidate loci in vision and pigmentation in the hamlets.

**Origin of Genomic Variants.** The old age (Fig. 1A) and high effective population size of the *Hypoplectrus* lineage (Fig. 3A) suggest that ancestral variation may have played an important role in the hamlet radiation. In order to test this hypothesis, we estimated the age of the genomic variants within our three regions

of interest. We used a nonparametric approach that combines probability distributions of the time to the most recent common ancestor of a large number of haplotypes, allowing us to estimate the age of genomic variants over a continuous timescale and without relying on a priori assumptions about demography or selection (55). We reasoned that the SNPs that are most strongly associated with the three phenotypic traits that we scored (spot on the snout, vertical bars, and saddle on the caudal peduncle) are the ones that are most likely to have a functional role and compared the strength of  $G \times P$  association with the estimated age of the derived allele for all the SNPs within our three candidate genomic regions. The results indicate that the majority of genomic variants that are strongly associated with each trait predate the radiation (i.e., are older than 10,000 generations), although a smaller number of younger variants also show strong associations (Fig. 6).

## Discussion

Hamlets live on coral reefs, a highly diverse and complex environment. They feed on small invertebrates and fishes (14, 56) but are not particularly specialized, and their 3-wk pelagic larval phase (10) provides potential for long-distance dispersal. Within this ecological backdrop, the hamlets show an extraordinary burst of speciation that is on par with radiations occurring in depauperate and geographically isolated environments. Moreover,

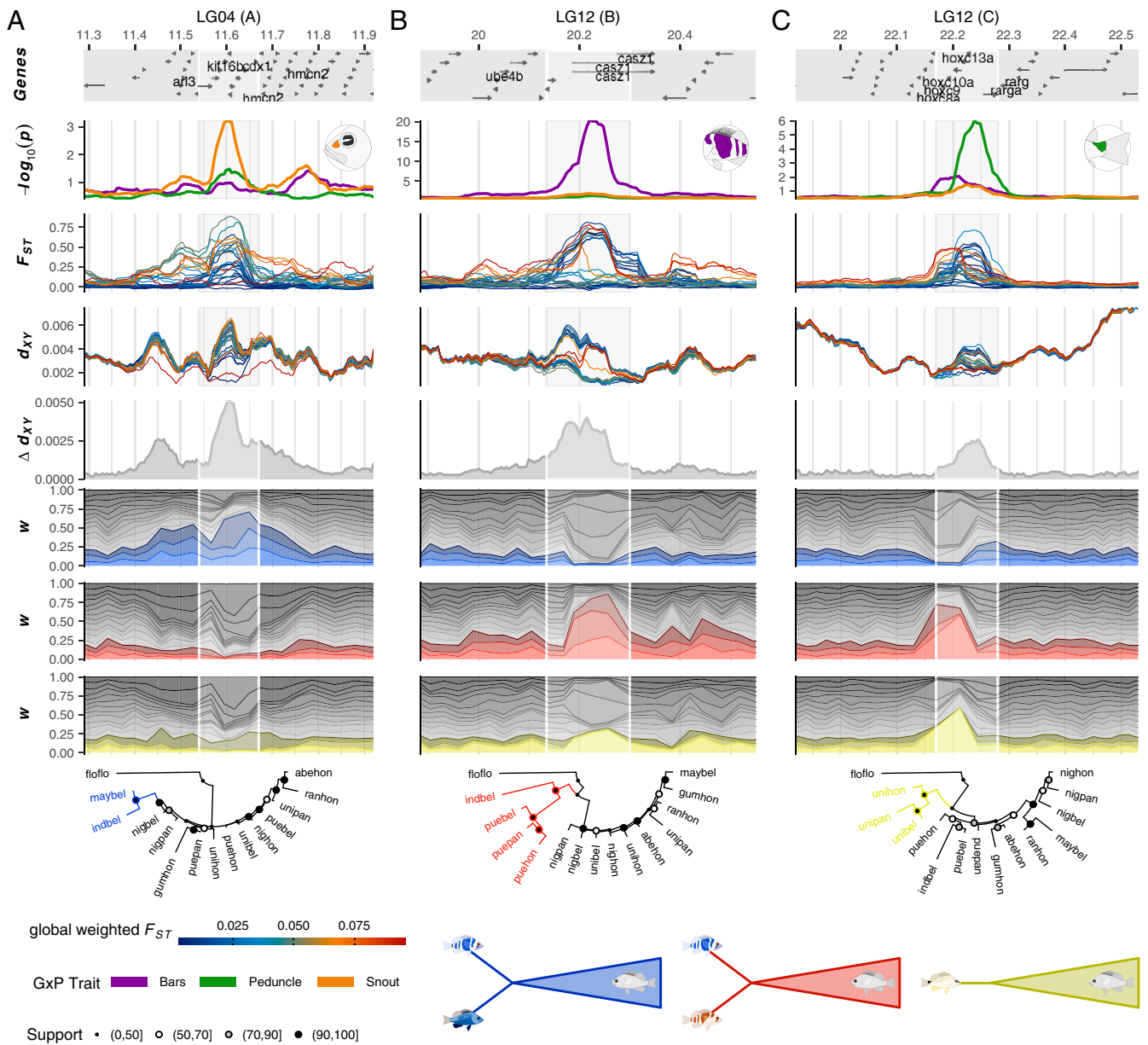


**Fig. 5.** Close-up views of three genomic regions of interest. A–C correspond to the A, B, and C regions, respectively, highlighted in Fig. 2. The x axis shows the position on the respective LG (in megabases), with regions above the 99.8th  $F_{ST}$  percentile highlighted in light gray. The first five subpanels correspond (from top to bottom) to the gene annotation, the log-transformed  $P$  value of the  $G \times P$  association, genetic differentiation ( $F_{ST}$ ), genetic divergence ( $d_{XY}$ ), and  $\Delta d_{XY}$  [ $\max(d_{XY}) - \min(d_{XY})$ ] among the 28 pairs of sympatric species color coded by genome-wide  $F_{ST}$ . All these statistics are calculated in 50-kb sliding windows with 5-kb increments. Note that the y scale varies between panels for  $G \times P$  association. The next three subpanels show the topology weighting for Belize, with particular sets of topologies highlighted. These correspond to the topologies in which the two blue species (*H. indigo* and *H. maya*) are sister species (blue), in which the two species with vertical bars (*H. indigo* and *H. puella*) are grouped together (red), and in which *H. unicolor* is sister to all other species (yellow). The last three subpanels show population-level phylogenetic trees of the regions above the 99.8th  $F_{ST}$  percentile highlighted in light gray. The first three letters of each sample indicate the species (*Hypoplectrus aberrans*, abe; *H. floridae*, flo; *H. gummigutta*, gum; *H. indigo*, ind; *H. maya*, may; *Hypoplectrus nigricans*, nig; *H. puella*, pue; *H. randallorum*, ran; and *H. unicolor*, uni), and the last three letters the location (Belize, bel; Honduras, hon; Panama, pan; and Florida, flo).

our genomic data suggest that diversification happened very recently and in a backdrop of substantial gene flow and introgression, resulting in a genetic architecture that is characterized by sharp peaks of differentiation. These peaks contain genes that are known to be involved in vision and pigmentation in other groups and suggest a modular architecture of color pattern variation in the group. Here, the term modular [or combinatorial (46)] refers to the observation that major patterning elements (e.g., vertical bars) and at least one color [black (25)]

are associated with one or a few genomic regions and that different species present different combinations of alleles at these loci. There is much more to be explored about the relationship between genomic and phenotypic variation in the hamlets, but such a modular architecture is similar to that observed in *Heliconius* butterflies (57), capuchino finches (58), and munia finches (59). These radiations also took place in diverse and complex environments and together with hamlets, provide the context for a more general understanding of the drivers of rapid speciation.

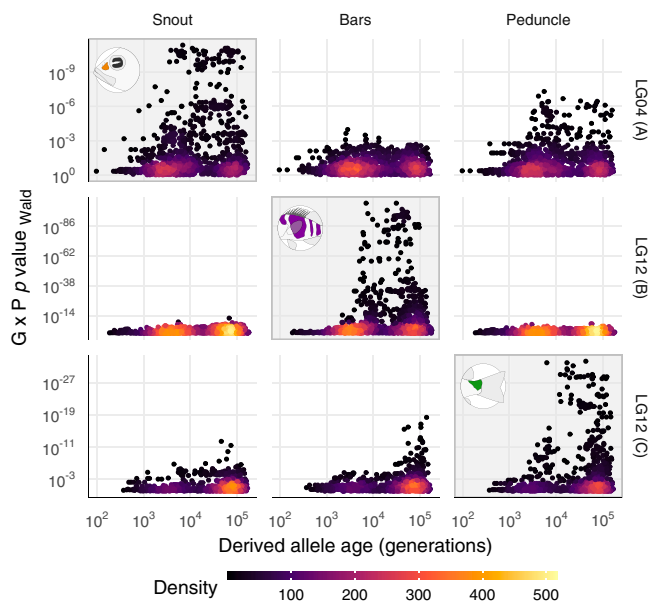


**Fig. 6.** Relationship between  $G \times P$  association and derived allele age in the three candidate regions. The three columns correspond to the three traits considered (vertical bars, spot on the snout, and saddle on the caudal peduncle), and the three rows correspond to the three candidate regions identified in Fig. 2. The highlighted panels correspond to the candidate interval for each trait. The color scale indicates the degree of overplotting of SNPs. Note the logarithmic scale on both axes and the different scales on the y axis. The other candidate regions are presented in *SI Appendix*, Fig. S19.

Color pattern is an important ecological trait that is under strong selection in tropical butterflies and finches (57–59). In the hamlets, the levels of hybridization and gene flow revealed by behavioral (10, 13, 18, 19, 21) and genetic (this study) analyses suggest that the phenotypic differences that define species should break down unless other factors prevent their homogenization. They do not, and hamlet species maintain their genetic and phenotypic integrity in sympatry. The role that particular color patterns play in survival and reproductive success remains a focus of study. The hamlets compete with a number of other predatory fishes on the reef (17) and are themselves prey to larger visual predators, such as groupers. In this context, any variation in color pattern that contributes to improving their hunting efficiency or survival is expected to be strongly selected for. Several hamlets have been suggested to be aggressive mimics (16, 17, 19, 20). From this perspective, ecological opportunity for radiation is not provided by a depauperate environment but on the contrary, is provided by strong competition and a high diversity of potential model species for aggressive mimicry. In addition, some pattern elements may play a role in camouflage, allowing individuals to both get closer to prey and avoid predation. For example, the vertical bars of the barred and indigo hamlets have been suggested to be cryptic in specific reef environments (17, 18). Cryptic color patterns are probably ancestral in the hamlets since these patterns are also observed in their closest relatives and in the sea basses (the Serranidae family) more generally. However, some hamlets have “almost gaudy” (17) color patterns that appear neither mimetic nor cryptic and might be more the result of sexual than natural selection. In this respect, the simultaneously hermaphroditic mating system of the hamlets can provide a strong source of sexual selection that is expected to facilitate the evolution of assortative mating among color morphs (13). Nevertheless, mating system alone cannot explain the hamlet radiation since no other serranine lineage that is also simultaneously hermaphroditic radiated explosively (Fig. 14).

In this light, our data also suggest that the hamlet radiation may have been further catalyzed by a tight coupling of loci involved in patterning and vision. The strongest and clearest signal in our data is the association between the presence/absence of vertical bars and genetic variation at the *casz1* locus. This transcription factor has been shown to be involved in the development of photoreceptors in mice (60, 61), and a role in vision is also likely in the hamlets since *casz1* is strongly and consistently expressed in the retinal tissue (25). The strong association with vertical bars that we report here suggests that *casz1*, or a locus in close proximity, might also be involved in patterning. This is similar to what has been observed in *Heliconius* butterflies, a system where strong natural and sexual selection acts on wing color patterns (62). The genetic basis of pattern variation is well characterized in this group, and recent work is demonstrating a tight physical linkage between loci responsible for color pattern variation and preferences for this variation (63). The possibility of physical linkage between patterning and sensory loci in hamlets is significant as it would both facilitate the evolution of reproductive isolation through visually-based assortative mating and help maintain it in the face of ongoing gene flow.

In any event, the occurrence of genes that are known to be involved in vision and pigmentation in peaks of differentiation is broadly in line with the genic view of speciation (64, 65), whereby differentiation between species is initially restricted to genes that are involved in reproductive isolation. Nevertheless, these highly differentiated regions do not expand with increasing genome-wide differentiation as predicted by this framework. This parallels what has been observed in *Heliconius* butterflies (66) and *Ficedula* flycatchers (38) and indicates that divergence hitchhiking does not play the prominent role in the buildup of genomic differences that is implied by the genic view of speciation in these groups. In the hamlets, this finding is consistent with the rapid decay of linkage disequilibrium along chromosomes (25, 45).

While marine systems are generally more open than terrestrial and freshwater habitats due to the scarcity of geographic barriers and the high mobility of many species (7), the hamlets remain nevertheless geographically constrained to the wider Caribbean. Within this region, they are essentially restricted to coral reefs, a highly discrete and patchy habitat. Their pelagic larval duration of 3 wk (10) is relatively short for a reef fish, and larval dispersal has been shown to be more restricted than previously thought in reef fishes generally (67) and in the hamlets in particular (68, 69). This explains the occurrence of local evolutionary processes (e.g., different levels of genetic clustering, differentiation, and hybridization) at our three study sites that are separated by just a few hundred kilometers. The hamlet lineage is also characterized by a history of high effective population size, which is typical of marine populations (11, 12, 70). This allows for both the accumulation of new genetic variants through mutation and the retention of ancestral genetic variants. While both ancestral and new variants are strongly associated with color pattern components, the majority of these variants predate the variation, pointing to an important role of ancestral variation.

We posit that the rapid hamlet radiation is driven by strong selection on color pattern, a modular genetic architecture for this trait, and a mating system that is conducive to the evolution of reproductive isolation among color morphs. Here, the historically high effective population size of hamlets provides a rich genomic substrate from which hybridization can rapidly assemble new phenotypic variation. This attribute is emerging as the common denominator to a variety of radiations on land and in the sea.

## Materials and Methods

**Software Versions, Parameter Settings, and Scripts.** Software versions and parameter settings were omitted from the text for readability; software versions are listed in *SI Appendix*. Data analysis was managed using nextflow (71). The workflows used to produce our results from raw data to figures are

provided in the accompanying repository [accessible from the accompanying repository (72) and the documentation therein; hereafter git].

**Sequencing.** This study is based on a total of 170 genomes obtained from 167 hamlets and three out-group samples ( $2 \times S. tortugarum$  and  $1 \times S. tabacarius$ ). Fifty genomes are new to this study, 110 are from ref. 25, and 10 are from ref. 45. All new tissue samples were available from previous studies (13, 19), except for sample #28393, which was collected in 2017 in Bocas del Toro (Panama) under the Smithsonian Tropical Research Institute Institutional Animal Care and Use Committee protocol 2017-0101-2020-2, the Panamanian Ministry of Environment permits SC/A-53-16 and SEX/A-35-17, and the Access and Benefit-Sharing Clearing-House identifier ABSCH-IRCC-PA-241203-1. Genomic DNA was extracted from gill tissue using Qiagen MagAttract High Molecular Weight kits. Libraries were prepared and sequenced by Novogene and the Institute of Clinical Molecular Biology (Kiel University) on an Illumina HiSeq 4000 (PE;  $2 \times 151$ ) to a mean postfiltering sequencing depth of  $17 \times$ .

**Variant Calling.** All the samples considered in this study were genotyped jointly and anew. The variant calling procedure was adapted from the best practice recommendations for the Genome Analysis Toolkit (GATK) workflow (73) provided by the Broad Institute (74, 75). The general workflow is presented below, and the exact parameters used for each step are provided in git 1.1 to 1.17 and 2.1 to 2.7. GATK was used to transform the sequences from fq to uBAM format, assign read groups, and mark adapters (git 1.2 to 1.4). The sequences were then back transformed to fq format using GATK, mapped to the hamlet reference genome using BWA (76), and merged with the uBAM files containing the read group information with GATK (git 1.5). Duplicated reads were removed (git 1.6), and genotype likelihoods were called for each individual (git 1.9) and then merged for all samples (git 1.10). All individuals were then genotyped jointly on the basis of the genotype likelihoods from all samples. This step was duplicated to create two versions of the dataset (git 1.11 and 2.4): a lightweight version with variant sites only (SNPs only; git 1.10) and a full version including every callable site—even invariant ones—to calculate  $\pi$  and  $d_{XY}$  (all base pairs [BP]; git 2.4). SNPs were extracted from the raw genotypes and hard filtered with respect to quality and missing data (git 1.14 and 2.6 to 2.7). The SNPs only dataset was also filtered for a minor allele count  $\geq 2$  and reduced to biallelic SNPs only using VCFtools (77) (git 1.14). In preparation of the phasing, the SNPs only dataset was subset by LG, and phase-informative reads were extracted based on the original alignments and the SNPs (git 1.15). Finally, genotypes were phased with SHAPEIT (78) (git 1.16 to 1.17). Bioinformatic phasing is notoriously difficult when it relies on population genetic data only (without, e.g., parent-offspring trios or linked reads). In order to mitigate this issue, we used the read-aware phasing approach implemented in SHAPEIT, which takes the phase information contained within the raw sequencing data into account. Demographic inference (see below) is the only analysis that relies on phase information.

**Serraninae Phylogeny and Speciation Rates.** To reconstruct the phylogenetic position of the hamlets within the Serraninae subfamily, we searched the *H. puella* reference genome for the 27 genes considered in the FTOL project (31) with Basic Local Alignment Search Tool (79) (23 of which were found; git 19.1 to 19.2). The corresponding regions were extracted from an unfiltered precursor genotype dataset of all BP, keeping only one high-coverage individual per species. Genotypes were converted to continuous sequence (Fasta format) using a custom Perl script and reverse complemented if necessary, and individual genes were aligned with MAFFT (80) to their FTOL homologs (git 19.3 to 19.6). Regarding the latter, only species in the Serraninae were retained, with species considered in the present study replacing original sequences. Ambiguously aligned positions were automatically removed with GBlocks (81), and minor adjustments were made by hand to finalize the mitochondrial gene alignments (we also dropped two poorly aligned genes in the two *Serranus* species altogether instead of manually editing them). Maximum likelihood reconstruction was performed with IQ-TREE (99) based on a concatenation approach with edge-linked partition model and 1,000 ultrafast bootstrap replicates (git 19.7). For divergence time estimates and evolutionary rate analysis, we used the time-calibrated FTOL phylogeny and Bayesian Analysis of Macroevolutionary Mixtures-estimated rates from the project's data repository (83). Tip-specific speciation rates ( $\lambda_{BAMM}$ ) were plotted for all ray-finned fish species included in the original data. These were then subset to the Serraninae subfamily, and mean speciation rates along the phylogeny were extracted using the R package BAMMtools. Clade-specific rates for hamlets and Serraninae excluding hamlets, the 95% credible set of rate shift configurations, and macroevolutionary rate cohorts were estimated following the BAMM documentation (git 20.8).

**Population Genetic Statistics.** Throughout the study, all windowed statistics were computed over 50-kb sliding windows with 5-kb increments unless stated otherwise.

**$F_{ST}$ .** Genetic differentiation was computed from the SNPs only dataset with VCFtools following Weir and Cockerham (84) and using the weighted mean. It was calculated within 50-kb windows for each species pair within each location (git 3.9) and among all groups (individual species within locations) jointly (git 3.7). The genome-wide weighted mean  $F_{ST}$  between populations of the same species was also calculated (git 3.21 to 3.24).

**$F_{ST}$  Permutation Test.** To test for significance,  $F_{ST}$  permutation tests were conducted for all pairs of sympatric species as well as for all pairs of allopatric populations of the same species. This was done genome wide for the SNPs only dataset as well as for a subset that excludes the regions above the 99.8th  $F_{ST}$  percentile (SI Appendix, Table S2, git 12.3 to 12.4), both filtered for a minor allele count of three (git 12.6). For a total of  $10^5$  iterations for each pair, the group assignment of the samples was permuted, and  $F_{ST}$  was computed (git 12.10 to 12.13). For each pair, the observed  $F_{ST}$  was then compared with the  $F_{ST}$  distribution derived from the permutations to compute an empirical  $P$  value. To account for multiple testing, the  $\alpha$  levels used as significance thresholds were adjusted following the modified false discovery rate procedure (85) (SI Appendix, Table S1).

**Principal Component Analysis.** Principal component analyses were conducted for each location using the R package SNPRelate (git 7.8 to 7.9). These were based on the SNPs only dataset filtered for minor allele count (git 7.7). Each principal component analysis was repeated on the whole genome as well as a subset that excludes the regions above the 99.8th  $F_{ST}$  percentile (SI Appendix, Table S2, git 7.4).

**$d_{XY}$ .** Genetic divergence (86) was computed from the all BP data within 50-kb windows. The data were reformatted to a custom genotype format, and divergence was computed using popgenWindows.py (87) (git 4.3 to 4.9).

**$\Delta d_{XY}$ .** This statistic, computed within 50-kb windows, was defined as the range of divergence among pairs of sympatric species:  $\Delta d_{XY} = \max(d_{XY}) - \min(d_{XY})$  among the 28 pairs.

**$\pi$ .** Nucleotide diversity was calculated for each hamlet group (species/population) within 50-kb windows (git 4.19) with popgenWindows.py using the all BP dataset.

**$G \times P$ .**  $G \times P$  associations were based on the SNPs only dataset and estimated using a linear model with GEMMA (88). This approach takes population structure into account by considering a matrix of relatedness among individuals. The dataset was transformed to the plink format using VCFtools and plink (89) (git 3.11 to 3.12).  $G \times P$  association was calculated on an SNP basis for the presence/absence of three phenotypic traits: vertical bars, saddle mark on the caudal peduncle, and spot on the snout (git 3.17). Phenotyping was based on photographs of all but five samples for which photographs were not available. A Wald test was conducted using GEMMA to determine the association between the phenotype and the genotype on a per SNP basis. The results were averaged over 50-kb windows (10 and 50 kb; git 3.20). Note that Wald test  $P$  values were  $-\log_{10}$  transformed before averaging, so  $-\log_{10}(p)$  is reported for every window. GEMMA was also run under the linear mixed model, which provided similar results (SI Appendix, Fig. S20).

**$\rho$ .** Population recombination rate ( $\rho$ ) was estimated using the R package FastEPRR (90). Briefly, this approach uses boosting (a machine learning approach) to select the best regression model between recombination rate and a set of summary statistics. The analysis was based on the SNPs only dataset considering all samples (except out-groups) and calculated within nonoverlapping windows of 50 kb using 250 parallel jobs (git 6.4 to 6.10). These results were also used to explore the correlation between  $\rho$ ,  $F_{ST}$ , and  $\pi$  with linear regression (SI Appendix, Figs. S6 and S9).

**$N_e$  and Cross-Coalescence Rate.** Demographic history was inferred using the multiple sequentially Markovian coalescent method implemented in MSMC2 (44). This analysis was based on the phased SNPs only dataset, which was prepared following the MSMC2 authors recommendations (91) as detailed in ref. 45. This included masking the data on the basis of mappability to the reference genome and the occurrence of indels. The data were also filtered with respect to coverage for each individual (between  $10 \times$  and twice the individual mean coverage; git 8.10). Individuals from each species and location were randomly grouped into sets of three or four, with each individual included in only one set (git 8.12), and individual masks were combined to create the MSMC2 input files (git 8.16 to 8.21). Individuals



were also grouped for the cross-coalescence rate analysis, with each group containing two individuals of each species for all pairs of sympatric species. Here, each individual was assigned to only one group for each species pair but reused across species pairs. All MSMC2 analyses were run with a time segmentation pattern of  $1 \cdot 2 + 25 \cdot 1 + 1 \cdot 2 + 1 \cdot 3$  and the average of Watterson's estimator across input datasets ( $\theta = 2.55 \cdot 10^{-3}$ ). The mutation rate was set to  $\mu = 3.7 \times 10^{-8}$  based on the closest relative for which we could find a reliable mutation rate estimate (91, 92) (git 8.18 and 8.23).

**Identification of Putative Hybrids and Backcrosses.** We used the approach implemented in NewHybrids (93) to evaluate ongoing gene flow among sympatric species. This method is based on patterns of Mendelian inheritance at highly differentiated loci. This analysis was based on small subsets of the SNPs only dataset. First, the 800 most differentiated SNPs were selected for each pair of sympatric species (git 9.5 to 9.6). These were then filtered for a minimum physical distance of 5 kb to reduce linkage among them using VCFtools (git 9.7). From this SNP set, 80 SNPs were randomly chosen using bash scripting and converted to the NewHybrids input format using PGDSpider (94). The assignment to hybrid classes with NewHybrids was implemented in the R package parallelnewhybrid (95), which was run with a burn-in of  $10^6$  iterations and  $10^7$  sweeps (git 9.8). Individuals with assignment to one hybrid class with a posterior probability  $>0.99$  were considered high-probability hybrids or backcrosses. The NewHybrids approach has the advantage of not requiring the a priori identification of pure individuals, but we note that it considers only one species pair at a time, ignoring the effect of other species on each pairwise analysis.

**D Statistics.** Levels of introgression among species/populations were assessed by applying Patterson's *D* (96) and related statistics. After removing all *Serranus* samples, the SNPs only dataset was filtered to exclude sites with linkage disequilibrium coefficients greater than 0.5 within 50-kb windows using the BCFtools (97) plug-in prune (git 17.1 to 17.4). Using the resulting 4,902,398 sites, *D* statistics were then calculated for all 364 population/species trios with Dsuite's Dtrios (98) using default parameters and *H. floridae* as the out-group. *P* values were adjusted for multiple testing using the Bonferroni procedure (git 17.5 to 17.8).

**Genome-Wide Hamlet Phylogeny.** To reconstruct the phylogenetic relationships among hamlets, we divided the genome into nonoverlapping windows of 5 kb. A total of 5,000 were selected randomly from those windows that contained less than 20% missing sites and at least 50 SNPs within hamlets in the all BP genotype dataset (69% of all windows met these criteria; git 13.1 to 13.11). The selected windows were extracted using VCFtools, and *Serranus* samples were removed in one copy of the dataset. After conversion to continuous sequence (Fasta format) using a custom Perl script, windows were individually realigned with MAFFT (80) (git 13.12 to 13.17). Maximum likelihood phylogenies were calculated for each window in IQ-TREE (82) based on the automatically selected best-fit model and default parameters (git 13.18). A coalescent-based species tree was then estimated from all local trees with ASTRAL-III (99), with internal branch length measured in coalescent units and support values given as local posterior probabilities (100) (git 13.19). Two species trees were produced that way, one rooted with *H. floridae* from the Gulf of Mexico clade and another one rooted with the three *Serranus* samples.

**Region-Specific Phylogenies.** The three genomic regions of interest were extracted from the all BP data (i.e., including invariant sites) set using VCFtools. All *Serranus* and hybrid samples identified by NewHybrids were removed alongside indel positions (git 14.1 to 14.3) before conversion to Fasta format and per site allele frequencies for each group using the cflib library. Region-specific phylogenies were then inferred at the level of individual samples with RAxML-NG (101) based on the GTR + G model, 10 each of random and parsimony starting trees, and 100 bootstrap replicates (git 14.5 to 14.6). Group-level maximum likelihood trees for each region were also estimated with IQ-TREE (82) using a polymorphism-aware model (102) and 100 nonparametric bootstrap replicates (git 14.4).

**Topology Weighting.** Topology weighting was conducted for Belize and Honduras independently (the number of taxa in Panama is too small to conduct this analysis). The SNPs only dataset was subset to include only hamlets from the respective location and filtered to include only SNPs with

a minor allele count greater than or equal to three (git 5.12). The data were then split by LG and converted to a custom genotype format (git 5.14). Using `phylml_sliding_windows.py` (87), we applied PhyML (103) to build phylogenies from nonoverlapping sliding windows of 200 SNPs each along all LGs (git 5.17). Topology weighting was conducted on the resulting phylogenies using Twisst (48) (git 5.18).

**IBD Fragments.** Fragments of IBD were identified using truffle (104). Out-group samples were removed from the SNPs only dataset with VCFtools (git 16.2), and truffle was run with three different minimum sequence length thresholds for IBD1 and IBD2 (25/20, 15/7.5, and  $10/5 \times 10^3$  consecutive SNPs; git 16.3 and 16.5). IBD fragment lengths were then converted from base pairs to centimorgans based on two available linkage maps for *Hypoplectrus* (42) (git 16.6). IBD networks were then constructed from the pairwise genome-wide average IBD [computed as  $(IBD2 + 0.5 \cdot IBD1)/(IBD0 + IBD1 + IBD2)$ ] as edge weights in a force-directed graph (105). In order to limit the effect of low recombination and stabilizing selection on the detection of IBD fragments, the IBD fragments that overlapped with regions of the genome above the 95th IBD score percentile (git 16.4 to 16.5) and that were smaller than 0.2 cM were also filtered out.

**Admixture Analysis.** We used admixture (106) to analyze the population genetic patterns at three genomic regions of interest. For this, the out-group species were removed from the dataset, and the genotypes were subset to the respective candidate regions and converted to plink format (git 10.4). Admixture was run for all *k* values between 2 and 15 for each region (git 10.6).

**Allele Age Estimation.** This was done using Genealogical Estimation of Variant Age, a nonparametric method that combines probability distributions of the time to the most recent common ancestor of a large number of haplotypes based on empirically constructed hidden Markov models to estimate the age of genomic variants over a continuous timescale and without relying on a priori assumptions about demography or selection (55). The ancestral state of all SNPs was determined using the *Serranus* out-groups and allele frequency (git 11.3). For SNPs that were invariant in both *S. tabacarius* and *S. tortugarum*, the *Serranus* allele was set as ancestral. For the SNPs that were variant within *Serranus*, the major allele was set as ancestral. The information about the ancestral state was added as an annotation to the vcf file (git 11.3) using `vcf-annotate`, and the vcf file was recoded using a custom java script in combination with Jvarkit (107) (git 11.4). GEVA was looped over the entire dataset in batches of 250 SNPs, with a mutation rate of  $3.7 \cdot 10^{-8}$  and an estimated effective population size of  $3 \cdot 10^5$ . Recombination rate was fixed at the average of each LG and based on the FastEPRR estimation, ranging from  $1.95 \cdot 10^{-10}$  to  $5.13 \cdot 10^{-10}$  (git 11.6). The results were then compiled for each LG (git 11.7).

**Visualization.** All results were plotted using R (git 20). The details of the visualization are provided in the R scripts and their documentation (git docs/index.html, file within the git repository). Other than the scripts within the GitHub repository, the visualization relied on the three custom R packages (hypogen, hypoimg, and GenomicOriginsScripts), which can also be accessed via GitHub (108). The R packages used are listed and referenced in *SI Appendix*. Package versions were managed using the R package `renv`; thus, the precise R configuration used for this study can be restored based on the provided lock file (git `renv.lock`, file within the git repository).

**Data Availability.** All raw sequencing data are deposited in the European Nucleotide Archive (project accession no. PRJEB35459). Whole-genome resequencing data, genotype data, population genetic summary statistics, and code used for data analysis have been deposited in Dryad (<https://doi.org/10.5061/dryad.280gb5mmt>) (109) and Zenodo (<https://doi.org/10.5281/zenodo.4709890> (72) and <https://doi.org/10.5281/zenodo.4709767>) (108). Individual sample accession numbers are provided in *SI Appendix, Table S3*.

**ACKNOWLEDGMENTS.** This study was funded by a grant from the Smithsonian Institute for Biodiversity Genomics and Global Genome Initiative Grants Program (to W.O.M., O.P., and C. Baldwin) and German Research Foundation Grant PU571/1–1 (to O.P.). We thank F. Coulmance, R. Burri, T. Gouhier, M. Heckwolf, B. M. Moran, R. Schneider, and M. Vargas as well as the Belizean, Honduran, and Panamanian authorities.

1. D. Schluter, *The Ecology of Adaptive Radiation* (Oxford Series in Ecology and Evolution, Oxford University Press, 2000).
2. S. Lamichhane *et al.*, Evolution of Darwin's finches and their beaks revealed by genome sequencing. *Nature* **518**, 371–375 (2015).
3. F. Ronco *et al.*, Drivers and dynamics of a massive adaptive radiation in cichlid fishes. *Nature* **589**, 76–81 (2021).

4. M. D. McGee *et al.*, The ecological and genomic basis of explosive adaptive radiation. *Nature* **586**, 75–79 (2020).
5. S. Poe *et al.*, Comparative evolution of an archetypal adaptive radiation: Innovation and opportunity in *Anolis* lizards. *Am. Nat.* **191**, E185–E194 (2018).
6. N. B. Edelman *et al.*, Genomic architecture and introgression shape a butterfly radiation. *Science* **366**, 594–599 (2019).

7. D. J. McCauley *et al.*, Marine defaunation: Animal loss in the global ocean. *Science* **347**, 1255641 (2015).
8. E. A. Fischer, Sexual allocation in a simultaneously hermaphroditic coral reef fish. *Am. Nat.* **117**, 64–82 (1981).
9. B. Holt, I. Côté, B. Emerson, Signatures of speciation? Distribution and diversity of *Hypoplectrus* (Teleostei: Serranidae) colour morphotypes. *Glob. Ecol. Biogeogr.* **19**, 432–441 (2010).
10. M. L. Domeier, Speciation in the serranid fish *Hypoplectrus*. *Bull. Mar. Sci.* **54**, 103–141 (1994).
11. J. L. Kelley, A. P. Brown, N. O. Therkildsen, A. D. Foote, The life aquatic: Advances in marine vertebrate genomics. *Nat. Rev. Genet.* **17**, 523–534 (2016).
12. J. A. Grummer *et al.*, Aquatic landscape genomics and environmental effects on genetic variation. *Trends Ecol. Evol.* **34**, 641–654 (2019).
13. O. Puebla, E. Bermingham, F. Guichard, Pairing dynamics and the origin of species. *Proc. Biol. Sci.* **279**, 1085–1092 (2012).
14. E. Whiteman, I. Côté, J. Reynolds, Ecological differences between hamlet (*Hypoplectrus*: Serranidae) colour morphs: Between-morph variation in diet. *J. Fish Biol.* **71**, 235–244 (2007).
15. B. G. Holt, B. C. Emerson, J. Newton, M. J. Gage, I. M. Côté, Stable isotope analysis of the *Hypoplectrus* species complex reveals no evidence for dietary niche divergence. *Mar. Ecol. Prog. Ser.* **357**, 283–289 (2008).
16. J. E. Randall, H. A. Randall, Examples of mimicry and protective resemblance in tropical marine fishes. *Bull. Mar. Sci.* **10**, 444–480 (1960).
17. R. E. Thresher, Polymorphism, mimicry, and the evolution of the hamlets (*Hypoplectrus*, Serranidae). *Bull. Mar. Sci.* **28**, 345–353 (1978).
18. E. A. Fischer, Speciation in the hamlets (*Hypoplectrus*: Serranidae): A continuing enigma. *Copeia* **1980**, 649–659 (1980).
19. O. Puebla, E. Bermingham, F. Guichard, E. Whiteman, Colour pattern as a single trait driving speciation in *Hypoplectrus* coral reef fishes? *Proc. Biol. Sci.* **274**, 1265–1271 (2007).
20. O. Puebla, S. Picq, J. S. Lesser, B. Moran, Social-trap or mimicry? An empirical evaluation of the *Hypoplectrus unicolor* - *Chaetodon capistratus* association in Bocas del Toro, Panama. *Coral Reefs* **37**, 1127–1137 (2018).
21. F. S. Barreto, M. A. McCartney, Extraordinary AFLP fingerprint similarity despite strong assortative mating between reef fish color morphospecies. *Evolution* **62**, 226–233 (2008).
22. E. A. Fischer, The relationship between mating system and simultaneous hermaphroditism in the coral-reef fish, *Hypoplectrus nigricans* (Serranidae). *Anim. Behav.* **28**, 620–633 (1980).
23. O. Puebla, E. Bermingham, F. Guichard, Perspective: Matching, mate choice, and speciation. *Integr. Comp. Biol.* **51**, 485–491 (2011).
24. E. Whiteman, M. Gage, No barriers to fertilization between sympatric colour morphs in the marine species flock *Hypoplectrus* (Serranidae). *J. Zool. (Lond.)* **272**, 305–310 (2007).
25. K. Hench, M. Vargas, M. P. Höppner, W. O. McMillan, O. Puebla, Inter-chromosomal coupling between vision and pigmentation genes during genomic divergence. *Nat. Ecol. Evol.* **3**, 657–667 (2019).
26. B. G. Holt, I. M. Côté, B. C. Emerson, Searching for speciation genes: Molecular evidence for selection associated with colour morphotypes in the Caribbean reef fish genus *Hypoplectrus*. *PLoS One* **6**, e20394 (2011).
27. O. Puebla, E. Bermingham, W. O. McMillan, Genomic atolls of differentiation in coral reef fishes (*Hypoplectrus* spp., Serranidae). *Mol. Ecol.* **23**, 5291–5303 (2014).
28. M. A. McCartney *et al.*, Genetic mosaic in a marine species flock. *Mol. Ecol.* **12**, 2963–2973 (2003).
29. M. L. Ramon, P. S. Lobel, M. D. Sorenson, Lack of mitochondrial genetic structure in hamlets (*Hypoplectrus* spp.): Recent speciation or ongoing hybridization? *Mol. Ecol.* **12**, 2975–2980 (2003).
30. E. Garcia-Machado, P. C. Monteagudo, M. Solignac, Lack of mtDNA differentiation among hamlets (*Hypoplectrus*, Serranidae). *Mar. Biol.* **144**, 147–152 (2004).
31. D. L. Rabosky *et al.*, An inverse latitudinal gradient in speciation rate for marine fishes. *Nature* **559**, 392–395 (2018).
32. B. E. Erisman, C. W. Petersen, P. A. Hastings, R. R. Warner, Phylogenetic perspectives on the evolution of functional hermaphroditism in teleost fishes. *Integr. Comp. Biol.* **53**, 736–754 (2013).
33. C. W. Petersen, Sexual selection and reproductive success in hermaphroditic seabasses. *Integr. Comp. Biol.* **46**, 439–448 (2006).
34. O. Puebla, E. Bermingham, F. Guichard, Population genetic analyses of *Hypoplectrus* coral reef fishes provide evidence that local processes are operating during the early stages of marine adaptive radiations. *Mol. Ecol.* **17**, 1405–1415 (2008).
35. S. Picq, W. O. McMillan, O. Puebla, Population genomics of local adaptation versus speciation in coral reef fishes (*Hypoplectrus* spp., Serranidae). *Ecol. Evol.* **6**, 2109–2124 (2016).
36. T. L. Turner, M. W. Hahn, S. V. Nuzhdin, Genomic islands of speciation in *Anopheles gambiae*. *PLoS Biol.* **3**, e285 (2005).
37. S. Renaut *et al.*, Genomic islands of divergence are not affected by geography of speciation in sunflowers. *Nat. Commun.* **4**, 1827 (2013).
38. R. Burri *et al.*, Linked selection and recombination rate variation drive the evolution of the genomic landscape of differentiation across the speciation continuum of *Ficedula* flycatchers. *Genome Res.* **25**, 1656–1665 (2015).
39. F. Han *et al.*, Gene flow, ancient polymorphism, and ecological adaptation shape the genomic landscape of divergence among Darwin's finches. *Genome Res.* **27**, 1004–1015 (2017).
40. S. Stankowski *et al.*, Widespread selection and gene flow shape the genomic landscape during a radiation of monkeyflowers. *PLoS Biol.* **17**, e3000391 (2019).
41. Y. Bourgeois, R. P. Ruggiero, J. D. Manthey, S. Boissinot, Recent secondary contacts, linked selection, and variable recombination rates shape genomic diversity in the model species *Anolis carolinensis*. *Genome Biol. Evol.* **11**, 2009–2022 (2019).
42. L. Theodosiou, W. O. McMillan, O. Puebla, Recombination in the eggs and sperm in a simultaneously hermaphroditic vertebrate. *Proc. Biol. Sci.* **283**, 20161821 (2016).
43. J. H. Gillespie, C. H. Langley, Are evolutionary rates really variable? *J. Mol. Evol.* **13**, 27–34 (1979).
44. S. Schiffels, R. Durbin, Inferring human population size and separation history from multiple genome sequences. *Nat. Genet.* **46**, 919–925 (2014).
45. B. M. Moran *et al.*, The evolution of microendemism in a reef fish (*Hypoplectrus maya*). *Mol. Ecol.* **28**, 2872–2885 (2019).
46. D. A. Marques, J. I. Meier, O. Seehausen, A combinatorial view on speciation and adaptive radiation. *Trends Ecol. Evol.* **34**, 531–544 (2019).
47. B. C. Victor, *Hypoplectrus floridae* n. sp. and *Hypoplectrus ecosur* n. sp., two new barred hamlets from the Gulf of Mexico (Pisces: Serranidae): More than 3% different in COI mtDNA sequence from the Caribbean *Hypoplectrus* species flock. *J. Ocean. Sci. Foundation* **5**, 1–19 (2012).
48. S. H. Martin, S. M. Van Belleghem, Exploring evolutionary relationships across the genome using topology weighting. *Genetics* **206**, 429–438 (2017).
49. S. Jeong, A. Rokas, S. B. Carroll, Regulation of body pigmentation by the Abdominal-B *Hox* protein and its gain and loss in *Drosophila* evolution. *Cell* **125**, 1387–1399 (2006).
50. S. V. Saenko, M. S. Marialva, P. Beldade, Involvement of the conserved *Hox* gene *Antennapedia* in the development and evolution of a novel trait. *EvoDevo* **2**, 9 (2011).
51. J. W. Poelstra, N. Vijay, M. P. Hoepfner, J. B. W. Wolf, Transcriptomics of colour patterning and coloration shifts in crows. *Mol. Ecol.* **24**, 4617–4628 (2015).
52. S. B. Carroll, J. K. Grenier, S. D. Weatherbee, *From DNA to Diversity, Molecular Genetics and the Evolution of Animal Design* (Blackwell Publishing Ltd, Oxford, United Kingdom, 2nd ed., 2005).
53. R. Thummel, L. Li, C. A. Tanase, M. Sarra, A. R. Godwin, Differences in expression pattern and function between zebrafish *hoxc13* orthologs: Recruitment of *Hoxc13b* into an early embryonic role. *Dev. Biol.* **274**, 318–333 (2004).
54. I. Jakovlić, W. M. Wang, Expression of *Hox* paralog group 13 genes in adult and developing *Megalobrama amblycephala*. *Gene Expr. Patterns* **21**, 63–68 (2016).
55. P. K. Albers, G. McVean, Dating genomic variants and shared ancestry in population-scale sequencing data. *PLoS Biol.* **18**, e3000586 (2020).
56. J. E. Randall, *Food Habits of Reef Fishes of the West Indies* (Institute of Marine Sciences, University of Miami Coral Gables, 1967).
57. S. M. Van Belleghem *et al.*, Complex modular architecture around a simple toolkit of wing pattern genes. *Nat. Ecol. Evol.* **1**, 52 (2017).
58. L. Campagna *et al.*, Repeated divergent selection on pigmentation genes in a rapid finch radiation. *Sci. Adv.* **3**, e1602404 (2017).
59. K. F. Stryjewski, M. D. Sorenson, Mosaic genome evolution in a recent and rapid avian radiation. *Nat. Ecol. Evol.* **1**, 1912–1922 (2017).
60. P. Mattar, J. Ericson, S. Blackshaw, M. Cayouette, A conserved regulatory logic controls temporal identity in mouse neural progenitors. *Neuron* **85**, 497–504 (2015).
61. P. Mattar, M. Stevanovic, I. Nad, M. Cayouette, *Cas2* controls higher-order nuclear organization in rod photoreceptors. *Proc. Natl. Acad. Sci. U.S.A.* **115**, E7987–E7996 (2018).
62. S. D. Finkbeiner, A. D. Briscoe, R. D. Reed, Warning signals are seductive: Relative contributions of color and pattern to predator avoidance and mate attraction in *Heliconius* butterflies. *Evolution* **68**, 3410–3420 (2014).
63. M. Rossi *et al.*, Visual mate preference evolution during butterfly speciation is linked to neural processing genes. *Nat. Commun.* **11**, 4763 (2020).
64. C. I. Wu, The genic view of the process of speciation. *J. Evol. Biol.* **14**, 851–865 (2001).
65. C. I. Wu, C. T. Ting, Genes and speciation. *Nat. Rev. Genet.* **5**, 114–122 (2004).
66. M. R. Kronforst *et al.*, Hybridization reveals the evolving genomic architecture of speciation. *Cell Rep.* **5**, 666–677 (2013).
67. G. P. Jones, *Mission Impossible: Unlocking the Secrets of Coral Reef Fish Dispersal in Ecology of Fishes on Coral Reefs*, C. Mora, Ed. (Cambridge University Press, Cambridge, United Kingdom, 2015), pp. 16–27.
68. O. Puebla, E. Bermingham, F. Guichard, Estimating dispersal from genetic isolation by distance in a coral reef fish (*Hypoplectrus puella*). *Ecology* **90**, 3087–3098 (2009).
69. O. Puebla, E. Bermingham, W. O. McMillan, On the spatial scale of dispersal in coral reef fishes. *Mol. Ecol.* **21**, 5675–5688 (2012).
70. R. S. Waples, Separating the wheat from the chaff: Patterns of genetic differentiation in high gene flow species. *J. Hered.* **89**, 438–450 (1998).
71. P. Di Tommaso *et al.*, Nextflow enables reproducible computational workflows. *Nat. Biotechnol.* **35**, 316–319 (2017).
72. K. Hench, M. Helmkamp, k-hench/hamlet\_radiation: PNAS revisions. Zenodo. <https://doi.org/10.5281/zenodo.4709890>. Deposited 22 April 2021.
73. A. McKenna *et al.*, The Genome Analysis Toolkit: A MapReduce framework for analyzing next-generation DNA sequencing data. *Genome Res.* **20**, 1297–1303 (2010).
74. M. A. DePristo *et al.*, A framework for variation discovery and genotyping using next-generation DNA sequencing data. *Nat. Genet.* **43**, 491–498 (2011).
75. G. A. Van der Auwera *et al.*, From FastQ data to high-confidence variant calls: The Genome Analysis Toolkit best practices pipeline. *Curr. Protoc. Bioinformatics* **43**, 11.10.1–11.10.33 (2013).
76. H. Li, R. Durbin, Fast and accurate short read alignment with Burrows-Wheeler transform. *Bioinformatics* **25**, 1754–1760 (2009).
77. P. Danecek *et al.*, 1000 Genomes Project Analysis Group, The variant call format and VCFtools. *Bioinformatics* **27**, 2156–2158 (2011).
78. O. Delaneau, J. Marchini, J. F. Zagury, A linear complexity phasing method for thousands of genomes. *Nat. Methods* **9**, 179–181 (2011).

79. W. Altschul, S. F. Adn Gish, W. Miller, E. Myers, D. Lipman, Basic local alignment search tool. *J. Mol. Biol.* **215**, 403–410 (1990).
80. K. Katoh, D. M. Standley, MAFFT multiple sequence alignment software version 7: Improvements in performance and usability. *Mol. Biol. Evol.* **30**, 772–780 (2013).
81. G. Talavera, J. Castresana, Improvement of phylogenies after removing divergent and ambiguously aligned blocks from protein sequence alignments. *Syst. Biol.* **56**, 564–577 (2007).
82. L. T. Nguyen, H. A. Schmidt, A. von Haeseler, B. Q. Minh, IQ-TREE: A fast and effective stochastic algorithm for estimating maximum-likelihood phylogenies. *Mol. Biol. Evol.* **32**, 268–274 (2015).
83. D. L. Rabosky *et al.*, Data from “An inverse latitudinal gradient in speciation rate for marine fishes.” Dryad. <https://datadryad.org/stash/dataset/doi:10.5061/dryad.fc71cp4>. Accessed 16 March 2021.
84. B. S. Weir, C. C. Cockerham, Estimating f-statistics for the analysis of population-structure. *Evolution* **38**, 1358–1370 (1984).
85. Y. Benjamini, D. Yekutieli, The control of the false discovery rate in multiple testing under dependency. *Ann. Stat.* **29**, 1165–1188 (2001).
86. M. Nei, *Molecular Evolutionary Genetics* (Columbia University Press, New York, NY, 1987).
87. S. H. Martin, Data from “genomics\_general: General tools for genomic analyses.” GitHub. [https://github.com/simonhmartin/genomics\\_general](https://github.com/simonhmartin/genomics_general). Accessed 18 March 2021.
88. X. Zhou, M. Stephens, Genome-wide efficient mixed-model analysis for association studies. *Nat. Genet.* **44**, 821–824 (2012).
89. S. Purcell *et al.*, PLINK: A tool set for whole-genome association and population-based linkage analyses. *Am. J. Hum. Genet.* **81**, 559–575 (2007).
90. F. Gao, C. Ming, W. Hu, H. Li, New software for the fast estimation of population recombination rates (FastEPRR) in the genomic era. *G3 (Bethesda)* **6**, 1563–1571 (2016).
91. S. Schiffels, Data from “msmc-tools: Tools and utilities for msmc and msmc2.” GitHub. <https://github.com/stschiff/msmc-tools>. Accessed 30 January 2019.
92. S. Liu, M. M. Hansen, M. W. Jacobsen, Region-wide and ecotype-specific differences in demographic histories of threespine stickleback populations, estimated from whole genome sequences. *Mol. Ecol.* **25**, 5187–5202 (2016).
93. E. C. Anderson, E. A. Thompson, A model-based method for identifying species hybrids using multilocus genetic data. *Genetics* **160**, 1217–1229 (2002).
94. H. E. L. Lischer, L. Excoffier, PGDSpider: An automated data conversion tool for connecting population genetics and genomics programs. *Bioinformatics* **28**, 298–299 (2012).
95. B. F. Wringe, R. R. E. Stanley, N. W. Jeffery, E. C. Anderson, I. R. Bradbury, Parallelnewhybrid: An R package for the parallelization of hybrid detection using NEWHYBRIDS. *Mol. Ecol. Resour.* **17**, 91–95 (2017).
96. N. Patterson *et al.*, Ancient admixture in human history. *Mol. Ecol. Resour.* **21**, 584–595 (2021).
97. P. Danecek *et al.*, Twelve years of samtools and bcftools. *Giga Sci.* **10**, giab008 (2021).
98. M. Malinsky, M. Matschiner, H. Svardal, Dsuite - fast d-statistics and related admixture evidence from vcf files. *Mol. Biol. Evol.* **36**, 1294–1301 (2019).
99. C. Zhang, M. Rabiee, E. Sayyari, S. Mirarab, ASTRAL-III: Polynomial time species tree reconstruction from partially resolved gene trees. *BMC Bioinformatics* **19** (suppl. 6), 153 (2018).
100. E. Sayyari, S. Mirarab, Fast coalescent-based computation of local branch support from quartet frequencies. *Mol. Biol. Evol.* **33**, 1654–1668 (2016).
101. A. M. Kozlov, D. Darrriba, T. Flouri, B. Morel, A. Stamatakis, RAxML-NG: A fast, scalable and user-friendly tool for maximum likelihood phylogenetic inference. *Bioinformatics* **35**, 4453–4455 (2019).
102. D. Schrempf, B. Q. Minh, A. von Haeseler, C. Kosiol, K. C. Polymorphism-aware species trees with advanced mutation models, bootstrap, and rate heterogeneity. *Mol. Biol. Evol.* **36**, 1294–1301 (2019).
103. S. Guindon *et al.*, New algorithms and methods to estimate maximum-likelihood phylogenies: Assessing the performance of PhyML 3.0. *Syst. Biol.* **59**, 307–321 (2010).
104. A. Dimitromanolakis, A. D. Paterson, L. Sun, Fast and accurate shared segment detection and relatedness estimation in un-phased genetic data via TRUFFLE. *Am. J. Hum. Genet.* **105**, 78–88 (2019).
105. T. M. J. Fruchterman, E. M. Reingold, Graph drawing by force-directed placement. *Softw. Pract. Exper.* **21**, 1129–1164 (1991).
106. D. H. Alexander, J. Novembre, K. Lange, Fast model-based estimation of ancestry in unrelated individuals. *Genome Res.* **19**, 1655–1664 (2009).
107. P. Lindenbaum, R. Redon, Bioalclidae, samjs and vcfilterjrs: Object-oriented formatters and filters for bioinformatics files. *Bioinformatics* **34**, 1224–1225 (2018).
108. K. Hench, k-hench/GenomicOriginsScripts: PNAS revisions. Zenodo. <https://doi.org/10.5281/zenodo.4709767>. Deposited 22 April 2021.
109. K. Hench, W. O. McMillan, O. Puebla, M. Helmkampf, Data from: Rapid radiation in a highly diverse marine environment. Dryad. <https://doi.org/10.5061/dryad.280gb5mmt>. Deposited 8 November 2021.